HHS Public Access

Author manuscript

Otol Neurotol. Author manuscript; available in PMC 2021 September 24.

Published in final edited form as:

Otol Neurotol. 2020 February ; 41(2): e280–e287. doi:10.1097/MAO.0000000000002491.

Anatomical and Functional Consequences of Microneedle Perforation of Round Window Membrane:

ANATOMICAL & FUNCTIONAL CONSEQUENCES OF RWM PERFORATION

Michelle Yu, BS[*], **Daniel N. Arteaga, BA**[*], **Aykut Aksit, MS**[†], **Harry Chiang, BA**[*], **Elizabeth S. Olson, PhD**[*,‡,§], **Jeffrey W. Kysar, PhD**[*,†,§], **Anil K. Lalwani, MD**[*,†,§]

[*]Department of Otolaryngology—Head and Neck Surgery, Columbia University Vagelos College of Physicians and Surgeons, New York, New York, U.S.A.

[†]Department of Mechanical Engineering, Columbia University, New York, New York, U.S.A.

[‡]Department of Biomedical Engineering, Columbia University, New York, New York, U.S.A.

[§]Co-Senior Authors

Abstract

Hypothesis: Microneedles can create microperforations in the round window membrane (RWM) without causing anatomic or physiologic damage.

Background: Reliable delivery of agents into the inner ear for therapeutic and diagnostic purposes remains a challenge. Our novel approach employs microneedles to facilitate intracochlear access via the RWM. This study investigates the anatomical and functional consequences of microneedle perforations in guinea pig RWMs *in vivo*.

Methods: Single 3D-printed, 100 μm diameter microneedles were used to perforate the guinea pig RWM via the postauricular sulcus. Hearing was assessed both before and after microneedle perforation using compound action potential and distortion product otoacoustic emissions. Confocal microscopy was used *ex vivo* to examine harvested RWMs, measuring the size, shape, and location of perforations and documenting healing at 0 hours (n = 7), 24 hours (n = 6), 48 hours (n = 6), and 1 week (n = 6).

Results: Microneedles create precise and accurate perforations measuring 93.1 ± 29.0 μm by 34.5 ± 16.8 μm and produce a high frequency threshold shift that disappears after 24 hours. Examination of perforations over time demonstrates healing progression over 24–48 hours and complete perforation closure by one week.

Conclusion: Microneedles can create a temporary microperforation in the RWM without causing significant anatomic or physiologic dysfunction. Microneedles have the potential to mediate safe and effective intracochlear access for diagnosis and treatment of inner ear disease.

Corresponding author: Anil K. Lalwani, MD, Division of Otology, Neurotology, and Skull Base Surgery, Department of Otolaryngology—Head and Neck Surgery, Columbia University College of Physicians and Surgeons, 180 Fort Washington Avenue, Harkness Pavilion, 8th Floor, New York, NY 10032, Phone: (212) 305-5820, anil.lalwani@columbia.edu.

Keywords

Round window membrane; Microneedle; Inner ear delivery; Hearing loss; Compound action potential; Otoacoustic emissions

INTRODUCTION

The cochlea is a closed structure almost entirely surrounded by bone. This restrictive anatomy presents a challenge in the treatment of inner ear diseases such as Ménière's Disease, sudden sensorineural hearing loss, and tinnitus—ailments that affect individuals of all ages and have a profound impact on quality of life (1). Current approaches to treatment of these disorders include systemic dosing and more direct delivery by cochleostomy. However, there are inherent disadvantages to these techniques: systemic dosing results in variable drug levels within the inner ear and is associated with systemic side effects, while cochleostomy breaches the delicate anatomy and risks damage to important structures (2–4).

The round window membrane (RWM), a thin layer of tissue separating the inner and middle ear compartments, is an attractive target for inner ear drug delivery (5). Intratympanic (IT) injection, the current standard of care, takes advantage of this portal into the inner ear and utilizes diffusion across the RWM to deliver therapy without manipulating cochlear anatomy (6,7). However, IT injection has drawbacks: diffusion of drug across the RWM varies with particle size and lipophilicity, contributing to unpredictable diffusion rates, inconsistent clinical results, and risk of hearing loss (8–12).

An elegant solution for reliable delivery to the inner ear is microperforation of the RWM, which has the potential to both increase the rate of diffusion and offer greater control over inner ear drug levels (13). Our laboratory has designed microneedles, based on the RWM's mechanical properties, geometry, and fibrous structure, to perforate the guinea pig RWM *in vitro* (14–16). Based on healing studies detailing the response to trauma in the inner ear, the RWM perforations were expected to fully close within one week and to have minimal effect on hearing (17,18).

This study investigates the anatomical and functional consequences of microperforation of the RWM *in vivo* through examination of perforation dimensions, perforation healing, and effects of RWM perforation on hearing.

MATERIALS AND METHODS

Microneedle Fabrication

Microneedles were fabricated using two-photon polymerization lithography by Photonic Professional GT system (Nanoscribe GmbH, Karlsruhe, Germany). The photoresist employed was IP-S (Nanoscribe GmbH). Each microneedle had a diameter of 100 μm, length of 150 μm, and an ultra-sharp tip with a tip radius of curvature of 500 nm, designed specifically to perforate the guinea pig RWM (14). The needle shafts were constructed with varying angles from vertical, including 0° and 30°, to accommodate variation in RWM surgical access. The needles were mounted to the ends of 30 gauge, blunt, stainless steel

syringe needles (Howard Electronic Instruments, El Dorado, Kansas) using commercial epoxy resin. Mounted needles were sterilized with ethylene oxide gas prior to survival surgeries. Each needle was used once.

Animals and Surgery

Columbia University Institutional Animal Care and Use Committee approved the care and use of the animals in this study. Twenty-seven adolescent male guinea pigs (Hartley strain) weighing 200 to 400 grams and age 1–6 weeks were obtained from a commercial vendor (Charles River, Inc., Massachusetts). Each guinea pig underwent surgery with RWM perforation (detailed below). The perforated RWM was harvested for analysis at one of four time points following the procedure (post-perforation): 0–2 hours (n = 7), 24 hours (n = 6), 48 hours (n = 6), and 1 week (n = 6). Experiments where the RWM was harvested 0–2 hours after surgery were non-survival surgeries and were used to evaluate perforation size and the reliability of the microneedle surgical technique. All other experiments were survival surgeries and were used to assess RWM healing over time (Fig. 1).

All surgeries were performed on the animal's right ear. The animals were anesthetized using isoflurane gas (induction at 3.0% and maintenance at 1.0–3.5%). Anesthesia depth was determined by respiratory status and toe pinch. Lidocaine was injected subcutaneously for local anesthesia. Body temperature was monitored by a probe placed under the animal's abdomen, and was maintained around 37 °C by a thermostatically controlled heating pad. For survival experiments, 0.5 mg/kg meloxicam and 1.0 mg/kg buprenorphine sustained release formula were administered as additional analgesics. The RWM was accessed via a postauricular incision and by creating a small opening through the skull into the bulla using a Stryker S2 πDrive drill (Stryker, Kalamazoo, Michigan). 2–3 mm of temporal bone were removed to expose and visualize the RWM. The surgical microneedle was secured onto a micromanipulator and was used to create a microscopic perforation in the RWM. Perforations were confirmed by one of several signs: visualization of the perforation, bleeding of the RWM, or pooling of perilymph in the round window niche and middle ear. Audiometric testing was conducted on the right ear at several time points during each experiment: 1) a baseline measurement after opening the bulla but prior to perforation, 2) 0–2 hours after perforation, and 3) immediately prior to RWM harvesting at 24 hours, 48 hours, or 1 week post-perforation. The animals were euthanized using pentobarbital overdose. The right temporal bone was extracted using blunt dissection and the RWM was fixed immediately with 10% buffered formalin. Three different researchers performed the non-survival surgery experiments and one researcher performed all survival surgery experiments.

Audiometric Testing

Compound action potential (CAP), which measures auditory nerve activity, and distortion product otoacoustic emissions (DPOAE), which measure outer hair cell health, were used to evaluate effects of microperforation on hearing. A silver ball electrode connected to a silver wire served as a CAP recording electrode and was positioned at the base of the cochlea bone. A reference electrode was placed subcutaneously 7–10 mm from the incision site and a ground electrode was placed subcutaneously between the shoulders. An AC amplifier

with a first order high pass filter and a second order low pass filter, with a pass band of ~200 Hz–4 kHz, was used to measure the CAP response. Sound stimulation was generated by a Tucker Davis Technologies (TDT) System (Tucker Davis Technologies Inc., Alachua, Florida) driving a Radio Shack dynamic speaker, connected in a closed-field configuration to the ear canal. Calibration of sound was performed within the ear canal using a Sokolich ultrasonic probe microphone. The CAP stimulus was composed of a 3 ms tone pip of variable frequency presented every 12 ms, with alternating polarity to eliminate the linear component of the cochlear microphonics from the averaged responses. CAP responses were collected for 18 frequencies ranging from 0.5 kHz to 40 kHz. Stimulus intensity was steadily increased in 5 dB increments to determine a hearing threshold. The threshold was defined as the lowest stimulus level that evoked a recognizable response curve. Experimenters were blinded to previous threshold measurements in order to minimize bias and error. CAP threshold shifts for each sampled time point and each frequency were considered significantly greater than zero at a threshold of $\alpha = 0.025$ using one-tailed paired t-tests. To measure DPOAE, a speaker and microphone held fixed to the ear canal were used to provide 70 dB sound stimuli with a fixed frequency ratio f2/f1 = 1.2 at 1 kHz increments between 1 kHz and 32 kHz and measure resulting distortion products from the ear.

Confocal Imaging of the RWM

Dissected, fixed temporal bones were washed with phosphate buffered saline (PBS) after one hour of fixation. Bony structures surrounding the cochlea were removed carefully using a Stryker S2 πDrive drill and forceps. The RWM was soaked in 1 mM rhodamine B (diluted in PBS), a fluorescent stain selective for elastic tissue (19), in PBS for 5 minutes, then rinsed with PBS three times and soaked in PBS for 15 minutes. Confocal imaging was performed with a Nikon A1R scanning confocal attachment on an Eclipse TiE microscope stand (Nikon Instruments, Melville, NY), using a 10x/0.45 Plan Apo or 20x/0.75 Plan Apo VC objective lens (Nikon). An excitation wavelength of 561 nm was chosen for the laser, and emitted light from 570 nm to 620 nm was allowed to pass to the detector. A stack of images was generated at several focal heights spaced 5 μm and 1 μm apart for the 10x objective and the 20x objective, respectively. At 10x magnification, the pinhole was set at 0.8 Airy unit (AU) to create an optical Z section of 6.35 μm; at 20x magnification, the pinhole was set at 0.9 AU to create an optical Z section of 2.3 μm.

Histology

RWM samples were fixed in 10% formalin immediately post-mortem for one hour and washed in PBS prior to imaging. Following imaging, samples were transferred to 70% ethanol. The remaining histological processing was performed at Molecular Pathology Shared Resource of the Herbert Irving Comprehensive Cancer Center of Columbia University. Samples were decalcified, paraffin-embedded, and cut into 5 μm sections. A Russell-Movat Pentachrome Stain was used to view connective tissue of the RWM.

SEM Imaging of Microneedles

After use in surgery, the microneedles were imaged using a scanning electron microscope (SEM) to examine for breaking and bending (Zeiss Sigma VP Scanning Electron Microscope).

Data Analysis

Confocal image analysis was conducted using ImageJ-Fiji software (20). Perforation sizes were measured using 0–2 hour post-perforation samples, based on a maximum intensity projection image. Measurements consisted of perforation area, major axis (an estimation of perforation length from corner to opposite corner), and minor axis (an estimation of perforation width approximately perpendicular to the major axis). Perforation closure over time was evaluated using a maximum intensity projection image and individual focal height images for each membrane. A perforation was considered open if the area within recognizable borders contained no fluorescence. The perforation was considered completely closed if the area within recognizable borders contained no areas lacking fluorescence. All other perforations were considered partially or incompletely closed.

RESULTS

Anatomical Consequences of RWM Perforation

Based on confocal images of RWM samples harvested at 0–2 hours post-perforation, perforations were fully open and lens-shaped, consistent with prior *in vitro* experiments (14) (Fig. 2A). The microneedles created perforations, measuring 93.1 ± 29.0 μm in the major axis and 34.5 ± 16.8 μm in the minor axis. The total perforation area averaged across all perforations measured 2572.3 ± 489.3 μm^2. Furthermore, all microneedles were intact and minimally bent after creating the perforations (Fig. 2B).

To investigate the longer-term anatomical effects of microneedle perforation, RWM samples harvested at later time points were examined for perforation closure (Fig. 3). At 24 hours, perforations appeared partially closed, with the original perforation shape still evident (Fig. 3B). In addition, a collection of tissue was observed within the area of the perforation at 24 hours (Fig. 3B). A pentachrome stain of histological sections confirmed the presence of blood cells and clumps of epithelial cells in the perforation area (Fig. 4). By 1 week, all harvested RWMs showed complete perforation closure with signs of reconstituted connective tissue fibers appreciated on 20x magnification images. There was little to no extra tissue or debris observed covering the perforation area (Fig. 3D). Perforations were not detectable in histologic sections at 48 hours or 1 week.

Functional Consequences of RWM Perforation

The effects of microneedle perforation on hearing were investigated using CAP and DPOAE. A mild CAP threshold shift of 5–10 dB from baseline was observed at 0–2 hours after surgery in the high frequency range from 22 to 40 kHz ($p < .025$) (Fig. 5A). At subsequent time points, no positive CAP threshold shifts were observed except for two frequencies at the lower bound of the testing range—1 kHz and 2 kHz—measured at 48 hours post-perforation ($p < .025$). Of note, there were negative CAP threshold shifts in the high frequency range observed in survival surgery time points, indicating improved hearing thresholds after perforation compared to baseline (Fig. 5). Examples of negative high frequency threshold shifts from individual 48-hour and 1-week experiments are shown in Figure 5B and 5C, respectively.

DPOAE is a measure of the cochlear condition and is due to the cochlea's active process, which originates in outer hair cells (21). All DPOAE measurements were well out of the noise level and were similar between baseline and post-perforation time points; a small DPOAE level increase can be seen in measurements from survival surgery time points (24 hours, 48 hours, and 1 week) compared to baseline (Fig. 6).

DISCUSSION

This study demonstrates that microneedles can accurately and precisely perforate the RWM *in vivo* without producing permanent major hearing loss; in addition, these perforations heal within one week. All guinea pig surgeries successfully produced RWM perforations that were comparable in size and shape to those produced *in vitro*: lens-shaped with an average major axis length approximately equal to microneedle shaft diameter of 100 μm (14). The minor axis and perforation area were also similar to measurements obtained *in vitro*. These results illustrate the repeatability of microperforations using the microneedles *in vivo*, even when performed by different investigators. In addition, due to the inherent constraints of performing *in vivo* surgery, the angles at which perforations were introduced differed from those performed under more controlled conditions *in vitro*. Nevertheless, the perforation sizes remained consistent, suggesting that variation in the angle of perforation does not affect perforation size. Importantly, the microneedles bent only minimally after perforating the RWMs. As such, they are well suited for use *in vivo* in guinea pigs. However, the long-term goals of this research include designing microneedles for use in humans. Because the human RWM is thought to be thicker than the guinea pig RWM, modifications to the microneedle design may be necessary (22,23).

The safety of microneedle perforation of the RWM was evaluated in this study by examining perforation healing and effects on hearing. Confocal imaging demonstrated that healing of guinea pig RWM microperforations begins within 24 hours with notable progress by 48 hours and complete closure by 1 week. This process occurs more quickly than in full RWM rupture, which has been observed to require two weeks for complete healing (17). Healing of RWM microperforations within a week is clinically important because it sets a time frame for drug diffusion across the microperforations. Moreover, while perilymph leakage may occur immediately following perforation, RWM healing prevents long-term leakage of perilymph from the inner ear (9,24). In the interim, a regenerative tissue matrix or hydrogel material—which has the capacity to carry therapeutic agents—may be considered to stymie perilymph leakage.

Beyond establishing a time frame for perforation healing, confocal images and histological sections also provided detailed insight into the healing process. At 24–48 hours, aggregated epithelial cells were visible in and around the perforations but by one week, these aggregates were no longer visible and the perforations were completely healed. In fact, by one week, perforations were often difficult to locate because the healed perforation areas appeared to have fibrous regrowth, resembling the surrounding un-perforated membrane. The healing of the RWM appears remarkably similar to the healing process described in the tympanic membrane, which also begins with epithelial migration followed by possible

fibrous regrowth (18,25–27). Future investigation into cell signaling and growth factors would help to elucidate the long-term healing of the RWM.

CAP and DPOAE measurements evaluated changes in hearing thresholds and outer hair cell health associated with RWM perforation, and demonstrated a temporary high frequency hearing loss that resolves within 24 hours. Of note, CAP measurements taken at least 24 hours after surgery indicate a negative threshold shift in the 20–40 kHz range. A similar phenomenon was observed in the DPOAE measurements, where survival surgery measurements were slightly higher than baseline measurements starting at 24 hours. It is likely that this threshold shift was a result of acoustic trauma from the surgery prior to measurement of baseline hearing; surgical access to the cochlea has been shown to cause temporary hearing loss in this range of 20–40 kHz in guinea pigs (28–30). As such, the results may underestimate the positive CAP threshold shifts in the high frequency range observed at 0–2 hours and the improved post-perforation CAP responses compared to the measured baseline may mask lasting hearing loss due to perforation. Without measurements of hearing prior to bone removal, small hearing changes that are lesser in magnitude compared to acoustic trauma from bone removal are undetectable. Likewise, CAP and DPOAE cannot detect effects of perforation on other aspects of cochlear performance, such as vestibular function. However, based on absolute thresholds, while a minor hearing loss cannot be ruled out, it can be concluded that no major hearing loss occurred due to RWM perforation.

In summary, microneedles can create precise perforations in the RWM *in vivo* that heal within one week. As such, microneedles provide an arsenal of new approaches to the management of inner ear diseases via the round window membrane—from diagnostic sampling of cochlear fluid to innovative therapies by drug diffusion or direct injection.

Acknowledgements:

The authors gratefully acknowledge support by the National Institutes of Health (NIH) National Institute on Deafness and Other Communication Disorders (NIDCD) with award number R01DC014547. The authors also thank Jimmy K. Duong for statistics consultation, Miguel Arriaga, Dimitrios Fafalis, and Wenbin Wang for productive discussions, Elika Fallah, Yi Wang, Elliot C. Strimbu, and Mohamed Diop for experiment consultation, Xun Wang and Karen Kasza, PhD for microscopy and experiment consultation, John Peregrin for histology consultation, Theresa C. Swayne and Emilia L. Munteaunu for assistance with microscopy, and the Columbia University Department of Otolaryngology—Head & Neck Surgery for use of the Temporal Bone Surgical Dissection Lab. Imaging was performed in the Confocal and Specialized Microscopy Shared Resource of the Herbert Irving Comprehensive Cancer Center at Columbia University, supported by NIH grant #P30 CA013696 (National Cancer Institute). The confocal microscope was supported by NIH grant #S10 RR025686.

Conflicts of Interest and Source of Funding:

Research was funded by the National Institutes of Health (NIH) National Institute on Deafness and Other Communication Disorders (NIDCD) with award number R01DC014547. Dr. Anil K. Lalwani is on the Medical Advisory Board of Advanced Bionics. For the remaining authors, no conflicts of interest were declared.

REFERENCES

1. Neuhauser HKThe epidemiology of dizziness and vertigo. Handb. Clin. Neurol137, 67–82 (2016). [PubMed: 27638063]
2. Borenstein JTIntracochlear drug delivery systems. Expert Opin. Drug Deliv8, 1161–1174 (2011). [PubMed: 21615213]

3. Peppi M, Marie A, Belline C & Borenstein JT Intracochlear drug delivery systems: a novel approach whose time has come. Expert Opin. Drug Deliv 15, 319–324 (2018). [PubMed: 29480039]
4. Liu H, Hao J & Li KS Current strategies for drug delivery to the inner ear. Acta Pharm. Sin. B 3, 86–96 (2013).
5. Goycoolea MV, Muchow D & Schachern P Experimental studies on round window structure: Function and permeability. Laryngoscope 98, 1–20 (1988).
6. Shemirani NL, Schmidt M & Friedland DR Sudden sensorineural hearing loss: An evaluation of treatment and management approaches by referring physicians. Otolaryngol. Neck Surg 140, 86–91 (2009).
7. Silverstein H, Lewis WB, Jackson LE, et al.Changing trends in the surgical treatment of Ménière's disease: results of a 10-year survey. Ear. Nose. Throat J82, 185–7, 191–4 (2003). [PubMed: 12696238]
8. Mikulec AA, Hartsock JJ & Salt AN Permeability of the Round Window Membrane Is Influenced by the Composition of Applied Drug Solutions and by Common Surgical Procedures. Otol. Neurotol 29, 1020–1026 (2008). [PubMed: 18758387]
9. Hahn H, Salt AN, Biegner T, et al.Dexamethasone levels and base-to-apex concentration gradients in the scala tympani perilymph after intracochlear delivery in the guinea pig. Otol. Neurotol33, 660–5 (2012). [PubMed: 22588238]
10. Goycoolea MVClinical aspects of round window membrane permeability under normal and pathological conditions. Acta Otolaryngol. 121, 437–47 (2001). [PubMed: 11508501]
11. Bremer HG, Rooy Ivan, Pullens B, et al.Intratympanic gentamicin treatment for Ménière's disease: a randomized, double-blind, placebo-controlled trial on dose efficacy - results of a prematurely ended study. Trials15, (2014).
12. Martin E & Perez N Hearing loss after intratympanic gentamicin therapy for unilateral Ménière's Disease. Otol. Neurotol 24, 800–6 (2003). [PubMed: 14501459]
13. Kelso CM, Watanabe H, Wazen JM, et al.Microperforations Significantly Enhance Diffusion Across Round Window Membrane. Otol. Neurotol36, 694–700 (2015). [PubMed: 25310125]
14. Aksit A, Arteaga DN, Arriaga M, et al.In-vitro perforation of the round window membrane via direct 3-D printed microneedles. Biomed. Microdevices20, 1–31 (2018).
15. Watanabe H, Cardoso L, Lalwani AK & Kysar JW A dual wedge microneedle for sampling of perilymph solution via round window membrane. Biomed. Microdevices 18, 24 (2016). [PubMed: 26888440]
16. Watanabe H, Kysar JW & Lalwani AK Microanatomic Analysis of the Round Window Membrane by White Light Interferometry and Microcomputed Tomography for Mechanical Amplification. Otol. Neurotol 35, 672–678 (2014). [PubMed: 24622022]
17. Gyo KHealing of experimentally produced round window membrane rupture. Acta Otolaryngol. 107, 85–9 [PubMed: 2929319]
18. Johnson AP, Smallman LA & Kent SE The mechanism of healing of tympanic membrane perforations. A two-dimensional histological study in guinea pigs. Acta Otolaryngol. 109, 406–15 [PubMed: 2360447]
19. Shelley WBFluorescent staining of elastic tissue with Rhodamine B and related xanthene dyes. Histochemie20, 244–249 (1969). [PubMed: 4190306]
20. Schindelin J, Arganda-Carreras I, Frise E, et al.Fiji: an open-source platform for biological-image analysis. Nat. Methods9, 676–682 (2012). [PubMed: 22743772]
21. Duifhuis HDistortion Product Otoacoustic Emissions: A Time Domain Analysis. ORL68, 340–346 (2006). [PubMed: 17065827]
22. Sahni RS, Paparella MM, Schachern PA, et al.Thickness of the Human Round Window Membrane in Different Forms of Otitis Media. Arch. Otolaryngol. - Head Neck Surg. 113, 630–634 (1987). [PubMed: 3566946]
23. Carpenter A-M, Muchow D & Goycoolea MV Ultrastructural Studies of the Human Round Window Membrane. Arch. Otolaryngol. - Head Neck Surg 115, 585–590 (1989). [PubMed: 2706104]

24. Plontke SK, Hartsock JJ, Gill RM, Salt AN. Intracochlear drug injections through the round window membrane: Measures to improve drug retention. Audiol Neurootol. 21(2): 72–79 (2016). [PubMed: 26905306]

25. Makuszewska M, Bonda T, Cieślińska M, et al.Expression of collagens type I and V in healing rat's tympanic membrane. Int. J. Pediatr. Otorhinolaryngol118, 79–83 (2019). [PubMed: 30590281]

26. Dong W, Stomackin G, Lin X, et al.Distortion product otoacoustic emissions: Sensitive measures of tympanic -membrane perforation and healing processes in a gerbil model. Hear. Res (2019). doi:10.1016/J.HEARES.2019.01.015

27. Tward;, C. DF.A.Cellular Dynamics in Early Healing of Mouse Tympanic Membranes. Otol. Neurotol40, 160–166 (2019).

28. Brown MC, Smith DI & Nuttall AL Anesthesia and surgical trauma: their influence on the guinea pig compound action potential. Hear. Res 10, 345–358 (1983). [PubMed: 6874605]

29. Honeder C, Ahmadi N, Kramer A-M, et al.Cochlear Implantation in the Guinea Pig. J. Vis. Exp (2018). doi:10.3791/56829

30. Suits GW, Brummett RE & Nunley J Second Place — Resident Clinical Science Award 1993: Effect of Otologic Drill Noise on ABR Thresholds in a Guinea Pig Model. Otolaryngol. Neck Surg 109, 660–667 (1993).

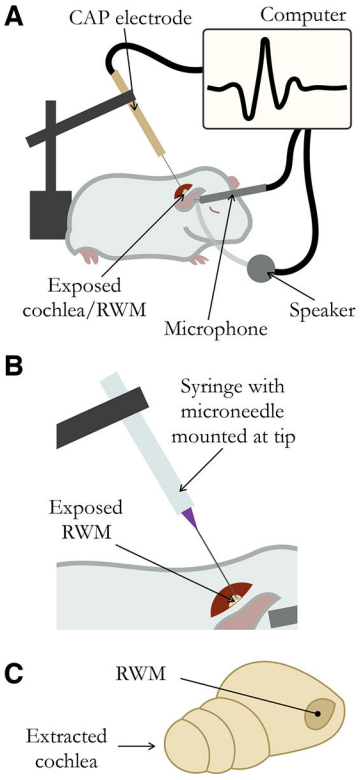

Surgically access cochlea

↓

Measure baseline hearing using **compound action potential (CAP)** and **distortion product otoacoustic emissions (DPOAE)**, shown in **A**

↓

Perforate the round window membrane (RWM) using a surgical microneedle mounted on a syringe, shown in **B**

↓

Re-measure hearing with CAP and DPOAE (**A**) immediately following perforation and prior to harvesting at various time points:

Non-survival surgery	0–2 hours	Measure perforation dimensions
Survival surgery	24 hours 48 hours 1 week	Follow perforation healing over time

↓

Fix and harvest the RWM, image and process for histology, shown in **C**

FIG. 1.

Flow diagram illustrating the experimental steps in order.

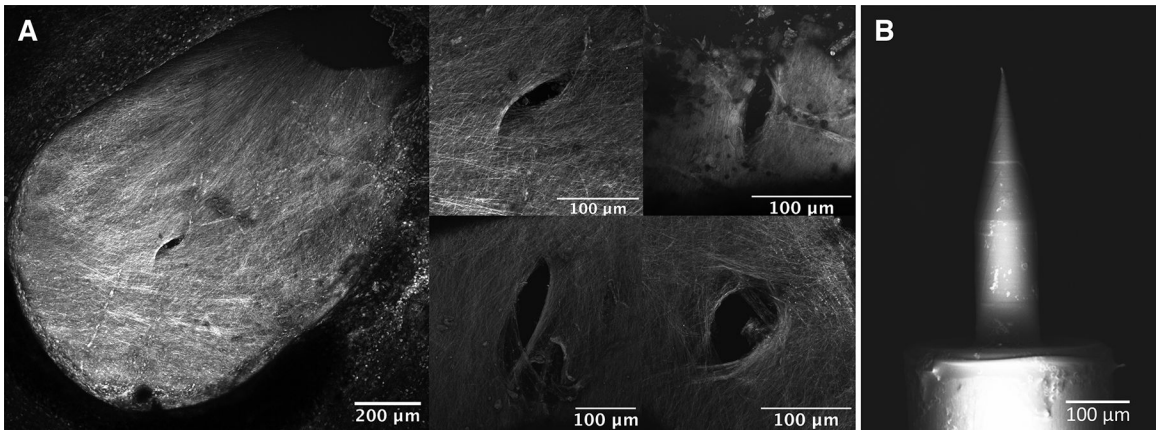

FIG. 2.

A, Confocal images of round window membranes (RWMs) perforated *in vivo*, harvested 0–2 hours after perforation. 10x magnification of a membrane is shown on left and 20x magnification of four separate perforations on different membranes is shown on right. *B*, Scanning electron microscope image of a microneedle after use in surgery.

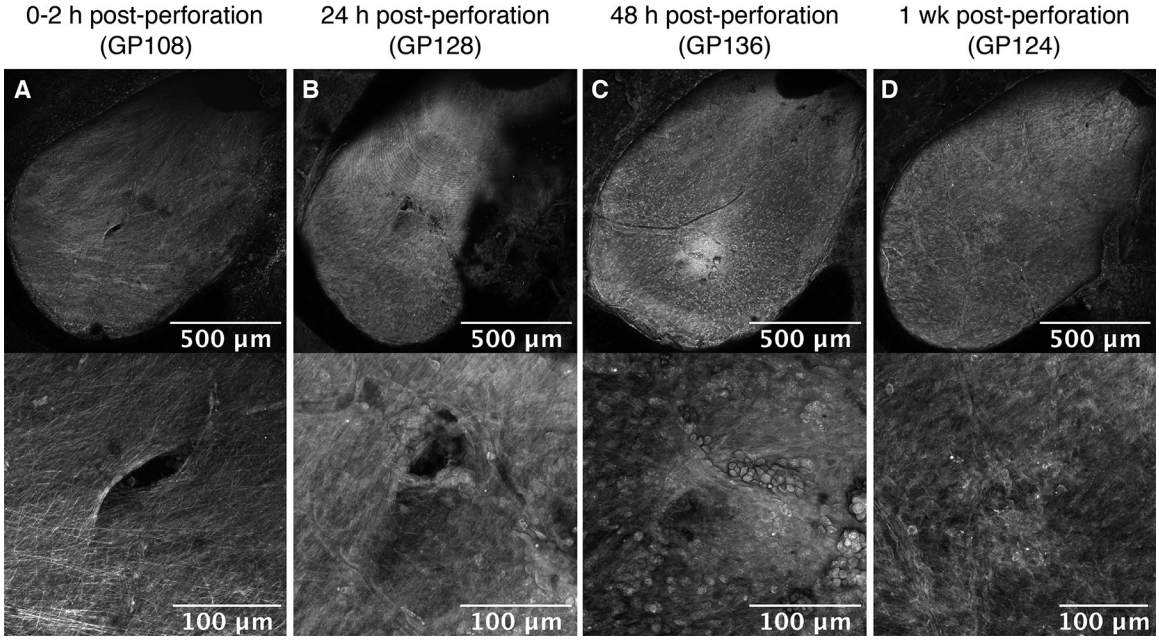

FIG. 3.

Round window membrane (RWM) healing over time. RWM perforations under 10x magnification (top) and 20x magnification (bottom) at (*A*) 0–2 hours, (*B*) 24 hours, (*C*) 48 hours, and (*D*) 1 week post-perforation, respectively.

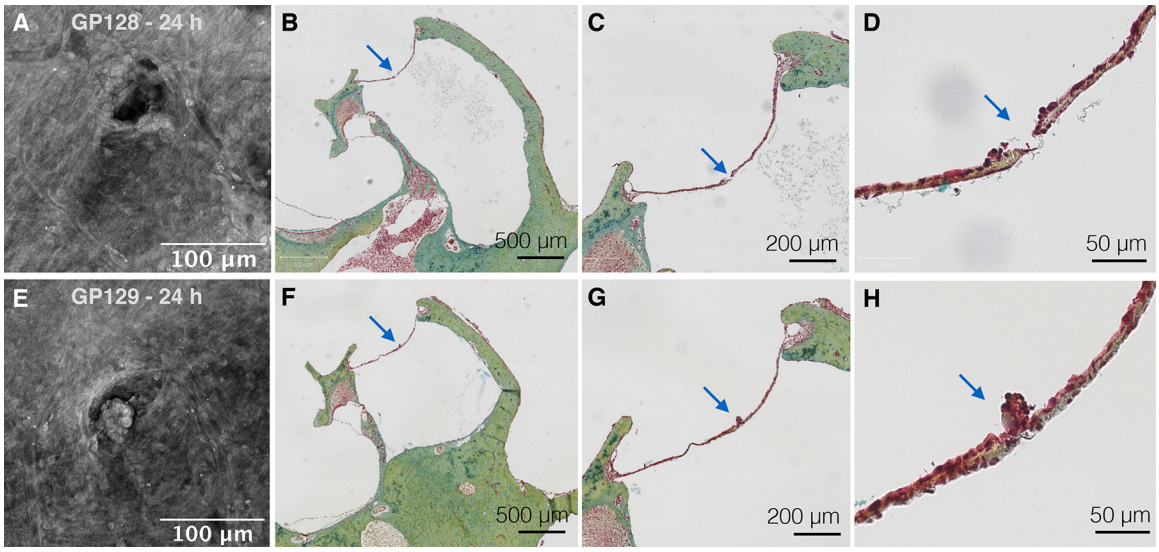

FIG. 4.

Confocal images of two perforation samples, 24 hours after perforation (*A* and *E*), shown with respective histologic sections using pentachrome stain (*B–D* and *F–H*). Arrows point at the perforation in each section. Epithelial cells are aggregated around perforation sites.

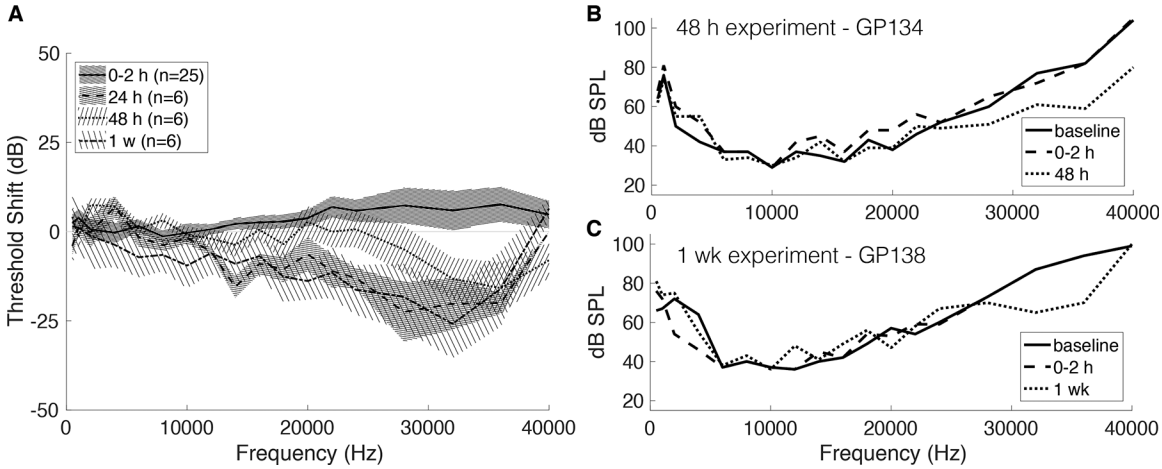

FIG. 5.

Using compound action potentials (CAPs) to evaluate hearing after perforation. *A*, Mean CAP threshold shift (compared to baseline) for each frequency, shown for all time points. Error bars are two times the standard error. There is a positive threshold shift at 0–2 hours in the 20 kHz to 40 kHz range, which recovers by 24 hours and becomes a negative threshold shift. *B*, Representative CAPs from a single 48-hour experiment, showing measurements at baseline, 0–2 hours after perforation, and 48 hours after perforation. *C*, Representative CAPs from a single 1-week experiment, showing measurements at baseline, 0–2 hours after perforation, and 1 week after perforation.

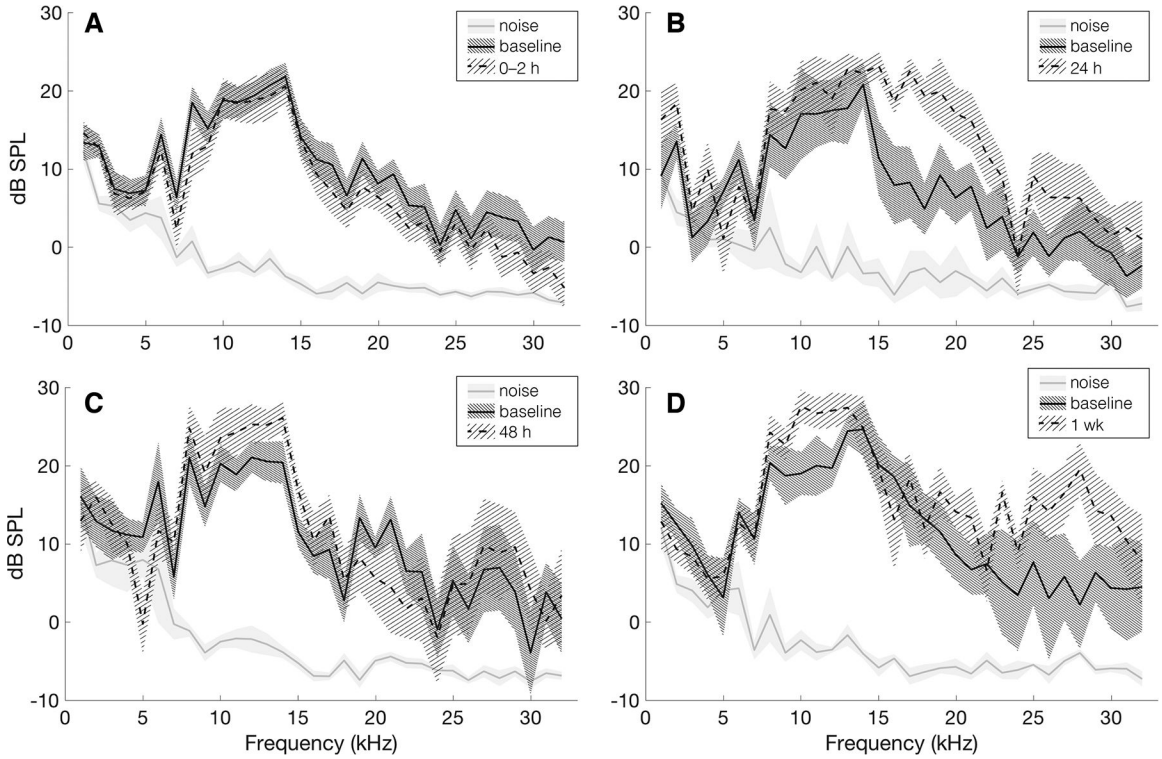

FIG. 6.

Distortion product otoacoustic emissions (DPOAE) at the frequency $2f1 - f2$ in response to a 70 dB stimulus over all survival experiments at 0–2 hours (*A*, n = 18), 24 hours (*B*, n = 6), 48 hours (*C*, n = 6), and 1 week (*D*, n = 6) post-perforation. Solid gray lines show average noise for the plotted experiments and the shaded gray area shows two times the standard error of the noise. Solid black lines show the mean measured baseline DPOAE signal and densely shaded areas show two times the standard error. Dotted lines show mean DPOAE signal for 0–2 h, 24 h, 48 h, and 1 wk experimental time points and lightly shaded areas show two times the standard error for respective experiments. All experiments show DPOAE signals out of the noise and similar pre- and post-perforation measurements.